coatings

MDPI

Article

Enhancing Perovskite Solar Cell Performance through Surface Engineering of Metal Oxide Electron-Transporting Layer

Gang Lu [1,2], Xuhui Wang [1], Juan Du [1], Min Zhang [1], Yali Gao [1], Yanbo Liu [1], Jing Ma [3] and Zhenhua Lin [3,*]

1 Qinghai Huanghe Upstream Hydropower Development Co. Ltd. Photovoltaic Industry Technology Branch, Photovoltaic Technology Co., Ltd. of Huanghe Hydropower, Xining 810000, Qinghai, China; eelugang@163.com (G.L.); wangxuhui@spic.com.cn (X.W.); dujuan@spic.com.cn (J.D.); zhangmin@spic.com.cn (M.Z.); gaoyali@spic.com.cn (Y.G.); liuyanbo@spic.com.cn (Y.L.)
2 Faculty of Automation and Information Engineering, Xi'an University of Technology, Xi'an 710048, China
3 State Key Discipline Laboratory of Wide Band Gap Semiconductor Tecchnology, Shaanxi Joint Key Laboratory of Graphene, School of Microelectronics, Xidian University, Xi'an 710071, China; 18710628890@163.com
* Correspondence: zhlin@xidian.edu.cn

Received: 23 November 2019; Accepted: 20 December 2019; Published: 3 January 2020

Abstract: Perovskite solar cells have gained increasing interest in recent times owing to the rapidly enlarged device efficiency and tunable optoelectronic properties in various applications. In perovskite solar cells, interface engineering plays an important role in determining the final device efficiency and stability. In this study, we adopted $TiCl_4$ treatment to reduce the surface roughness of the metal oxide layer and improve the perovskite film quality to obtain better device performance. After proper $TiCl_4$ treatment, the efficiencies of $TiCl_4$–TiO_2- and $TiCl_4$–ZnO-based devices were significantly enhanced up to 16.5% and 17.0%, respectively, compared with those based on pristine TiO_2 and ZnO (13.2% and 10.2%, respectively).

Keywords: perovskite solar cells; $TiCl_4$ treatment; electron-transporting layer; interface engineering

1. Introduction

Perovskite solar cells (PSCs) have attracted continuously increased interest owing to their unique properties and high performance [1–10]. In order to further enhance device efficiency and stability, some additional interface and compositional engineering approaches are necessary [11–18]. Some interface engineering approaches have previously been investigated to optimize energy level alignment and relieve charge accumulation [19–21]. Generally, for interface transport layers, a high-quality film with properties including sufficient charge extraction capability, good film conductivity, and proper energy level should be guaranteed [19,22]. Hence, various interface transporting layers have been studied. Among them, metal oxides (e.g., ZnO, SnO_2, and TiO_2) have been widely investigated as electron-transporting layers (ETLs) in PSCs [23–37], particularly TiO_2 ETL. The surface and electronic properties of TiO_2 play important roles in determining the final device performance, including power conversion efficiency (PCE), hysteresis behavior, and stability [20,38,39]. In order to enhance device performance and reduce hysteresis behaviors encountered in TiO_2-based devices, various techniques have been used to optimize the TiO_2 surface or electronic properties. This includes the addition of fullerene molecules, amino acids, or C60-SAM, which are commonly applied to optimize the charge transfer process [28,29,40,41]. Besides this, $TiCl_4$ soaking treatment has been investigated in dye-sensitized solar cells to enhance device performance [42]. $TiCl_4$ treatment has also been

applied in PSC devices to fill the voids at the TiO_2/perovskite layer interfaces and smooth the TiO_2 surface [39,43,44].

In this study, to investigate the mechanism of $TiCl_4$ and the role it plays with TiO_2 and phenyl-C61-butyric acid methyl ester (PCBM) in PSCs, we investigated the effects of $TiCl_4$ treatment on the quality of perovskite thin film and the corresponding device performance. Results showed that, after $TiCl_4$ treatment, the perovskite film quality was significantly enhanced; moreover, the charge transfer and extraction became more efficient. Finally, compared to pristine TiO_2- and ZnO-based devices (13.2% and 10.2%), the efficiencies of both $TiCl_4$–TiO_2- and $TiCl_4$–ZnO-based devices were significantly improved up to 16.5% and 17.0%, respectively, with simultaneously enhanced open-circuit voltage (V_{oc}), short-circuit current density (J_{sc}), and fill factor (FF).

2. Results and Discussion

Surface morphologies of ETLs with and without $TiCl_4$ treatment were investigated by tapping-mode atomic force microscopy (AFM) (Dimension Icon AFM, Bruker, Billerica, MA, USA). The surface roughness of the TiO_2 surface decreased from 18.0 to 13.9 nm after $TiCl_4$ treatment (Figure 1). After depositing the PCBM layer, the surface roughness was maintained without much change. This indicates that the surface roughness is mainly determined by $TiCl_4$ treatments. These properties may affect perovskite crystallization and formation as well as the crystal size.

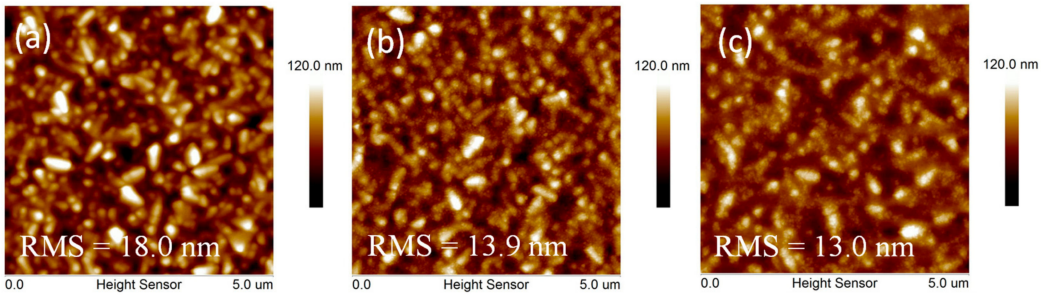

Figure 1. Atomic force microscopy (AFM) images of (**a**) pristine TiO_2 electron-transporting layer (ETL), (**b**) with $TiCl_4$ treatment, and (**c**) with $TiCl_4$ and PCBM treatment.

The energy levels of TiO_2/PCBM electron-transporting layers with and without $TiCl_4$ treatment were investigated by ultraviolet photoelectron spectroscopy (UPS) (Escalab 250Xi, Thermo Scientific, Waltham, MA, USA). In Figure 2, it can be seen that the TiO_2/PCBM work function decreased from 4.18 to 4.09 eV after $TiCl_4$ treatment. The decreased work function would result in better energy level alignment and more efficient electron transfer between the conduction band of perovskite and the Fermi level of ETL. Moreover, the potential difference between two electrode contacts, such as TiO_2 and spiro-OMeTAD, was also enlarged due to the decreased work function, hence increasing the V_{oc} of the device [33].

In order to illustrate the effect of $TiCl_4$ treatment on the properties of perovskite thin film, the thin film morphologies of the perovskites upon ETLs with and without $TiCl_4$ treatment were investigated. As shown in Figure 3, the perovskite crystal size was enhanced, indicating a favorable crystal growth process on the $TiCl_4$-treated surface, which may have been caused by the low surface roughness value. The improved crystalline quality was also confirmed by the XRD patterns. As shown in Figure 4, strong diffraction intensity at around 14.6°, 28.9°, and 32.3° were observed and assigned to (110), (220), and (310) crystal planes of tetragonal perovskite phase, respectively. The diffraction pattern at 13.1° originated from PbI_2 because of the excess PbI_2 over CH_3NH_3I. These results are consistent with those previously reported [8,9]. Moreover, the diffraction intensity of the perovskite thin films with additional $TiCl_4$ treatment exhibited slight enhancement. This indicates that the thin film crystallinity was increased, resulting in more efficient charge transport and collection.

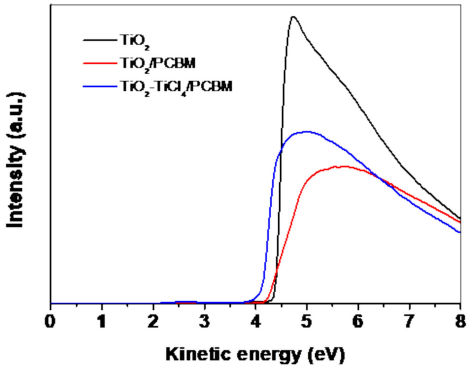

Figure 2. Ultraviolet photoelectron spectroscopy (UPS) spectra of ETL layers with and without $TiCl_4$ treatment.

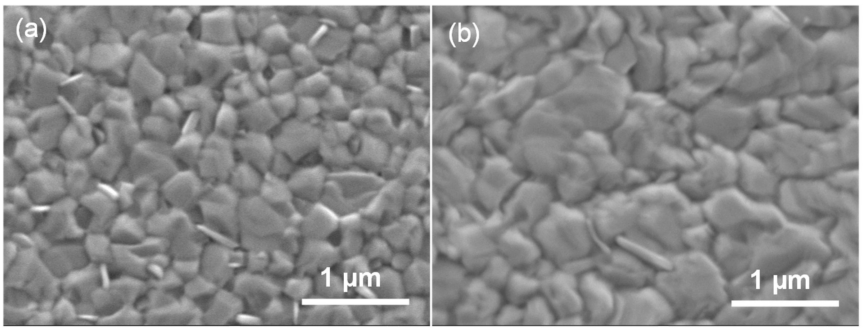

Figure 3. SEM images of perovskite films deposited on TiO_2 **(a)** and $TiCl_4$-treated TiO_2 ETLs **(b)**.

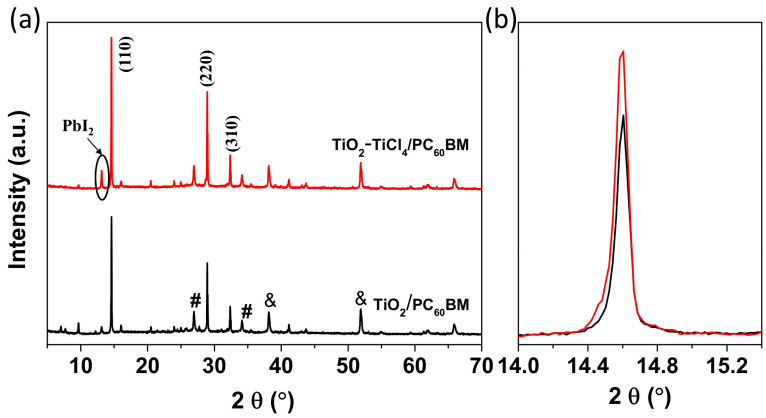

Figure 4. XRD patterns (**a**) and zoomed-in XRD patterns (**b**) of perovskite films deposited on TiO_2 and $TiCl_4$-treated TiO_2 ETLs. "#" and "&" represent the characteristic peaks of fluorine-doped tin oxide (FTO) and TiO_2, respectively.

The film absorption spectra of perovskite films deposited on TiO_2 and $TiCl_4$-treated ETLs were investigated by UV–Vis spectroscopy. Both films exhibited high absorption intensity over the entire UV–visible range, and the absorption band edge was around 1.61 eV (Figure 5). Compared with pristine TiO_2 ETL, the absorption of the perovskite film based on $TiCl_4$-treated TiO_2 ETL was significantly enhanced, indicating enhanced crystallinity of the resulting thin film.

To further investigate the photophysical properties of the thin films, steady-state photoluminescence (PL) and time-resolved PL (TR-PL) measurements of perovskite thin films were further investigated. The perovskite film based on $TiCl_4$-treated TiO_2 ETL showed larger PL intensity decay compared to the pristine TiO_2-based perovskite film (Figure 6), indicating a faster charge transfer

process between TiO_2 and perovskite thin films [30]. Furthermore, the PL lifetimes of perovskite films on glass were also measured (Figure 7). By fitting the TR-PL curves with biexponential function, two decay parts—fast decay and slow decay—could be obtained [14]. The average lifetimes derived from the fitting curves were around 25.7 and 29.8 ns for perovskite films with and without $TiCl_4$ treatment, respectively. The decreased PL lifetime is related to the efficient charge carrier transfer induced quenching process [27]. This is essential for efficient charge extraction and collection of the device.

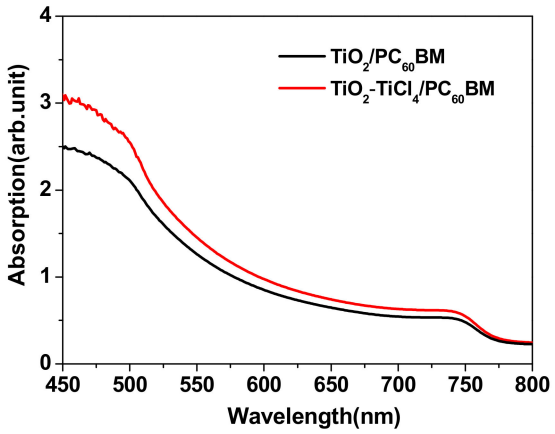

Figure 5. UV–vis spectra of perovskite films deposited on TiO_2 and $TiCl_4$-treated TiO_2 ETLs.

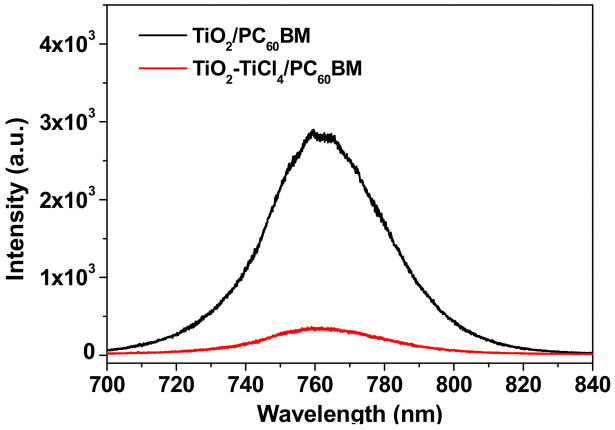

Figure 6. Photoluminescence (PL) spectra of perovskite films deposited on TiO_2 and $TiCl_4$-treated TiO_2 ETLs.

The effect of $TiCl_4$ treatment on PSC device performance was studied based on a planar structure with a configuration of FTO/TiO_2/$PC_{60}BM$/$CH_3NH_3PbI_{3-x}Cl_x$/spiro-OMeTAD/Ag. Figure 8 exhibits the current density − voltage ($J - V$) curves of PSC devices with and without $TiCl_4$ treatment, and Table 1 summarizes the corresponding device parameters. In Figure 8, a PCE of 13.2% (V_{oc} of 1.04 V, J_{sc} of 19.1 mA/cm^2, and FF of 0.66) can be seen for the device with pristine TiO_2. By comparison, all the parameters, i.e., V_{oc}, J_{sc}, and FF, for the device with $TiCl_4$ treatment were enhanced simultaneously, resulting in an improved average PCE of 16.5% (V_{oc} of 1.08 V, J_{sc} of 22.4 mA/cm^2, and FF of 0.68). The device series resistance (R_s) and shunt resistance (R_{sh}) were also calculated to further understand the improvement in performance. Compared to the device without $TiCl_4$ treatment, the R_s value of the device with $TiCl_4$ treatment decreased to 3.7 Ω·cm^2, while the R_{sh} increased to 6.9 kΩ·cm^2. The decreased R_s and increased R_{sh} are responsible for the J_{sc} and FF enhancement [7]. It needs to be mentioned that, when the high-temperature TiO_2 was replaced with the low-temperature ZnO layer, the device also showed similar improvement. The ZnO with $TiCl_4$ treatment revealed an improved

PCE of 17.0% with a V_{oc} of 1.08 V, J_{sc} of 23.2 mA/cm^2, and FF of 0.67, which was much higher than those of the device with pristine ZnO.

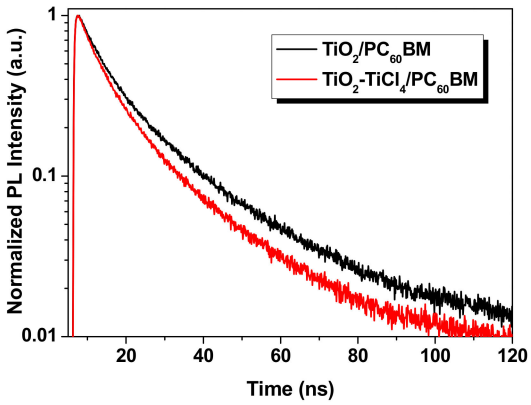

Figure 7. Time-resolved PL (TR-PL) spectra of perovskite films deposited on TiO_2 and $TiCl_4$-treated TiO_2 ETLs.

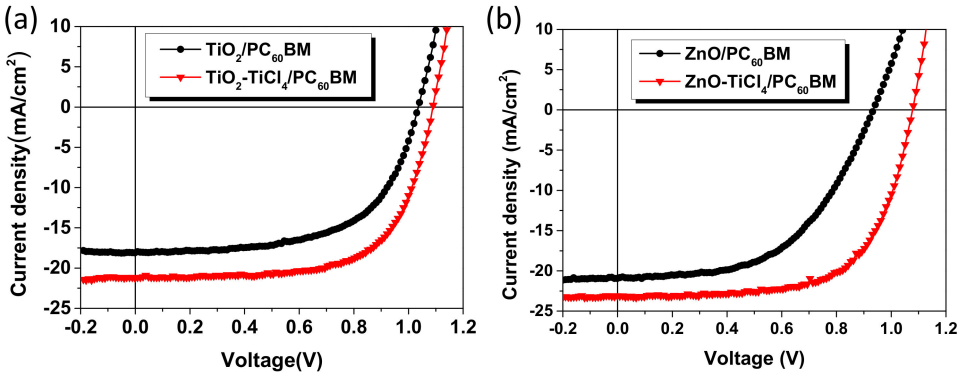

Figure 8. Current density − voltage ($J-V$) characteristics of devices based on TiO_2 (**a**) and ZnO (**b**) ETLs with and without $TiCl_4$ treatment.

Table 1. Device parameters of perovskite solar cells (PSCs) with and without $TiCl_4$ treatment.

Interlayer	V_{oc} (V)	J_{sc} (mA/cm^2)	FF	PCE (%)	R_s (Ω cm^2)	R_{sh} (kΩ cm^2)
TiO_2/PCBM	1.04	19.1	0.66	13.2	5.9	4.1
TiO_2–$TiCl_4$/PCBM	1.08	22.4	0.68	16.5	3.7	6.9
ZnO/PCBM	0.93	20.7	0.53	10.2	10.2	1.5
ZnO–$TiCl_4$/PCBM	1.08	23.2	0.67	17.0	5.1	2.8

The device hysteresis behavior is also a significant parameter to determine the final performance of the device. It can be affected by many factors, such as carrier trapping, ion motion, charge accumulation at interfaces, and so on [45–48]. The device hysteresis behaviors under different scan directions were measured (Figure 9). The device did not exhibit serious hysteresis behavior before and after $TiCl_4$ treatment, indicating that $TiCl_4$ has less effect than PCBM, which plays a major role in determining the final hysteresis behavior.

In order to further investigate the mechanism involved in performance enhancement, transient photocurrent and photovoltage measurements of perovskite solar cells were performed. Figure 10a shows the transient photocurrent decay of perovskite devices measured at short-circuit condition. After $TiCl_4$ treatment, the devices exhibited faster decay with shorter lifetime (1.02 μs) compared to the pristine TiO_2-based device (1.78 μs). This indicates that the device with $TiCl_4$ treatment possessed more efficient charge transfer process. The transient photovoltage was used to determine the charge

recombination process (Figure 10b). It can be clearly seen that the device with $TiCl_4$ treatment exhibited much longer lifetime (2.32 ms) compared to the pristine TiO_2-based device (1.66 ms). This indicates that the charge recombination process was efficiently suppressed. Hence, the J_{sc} and FF exhibited significant improvement.

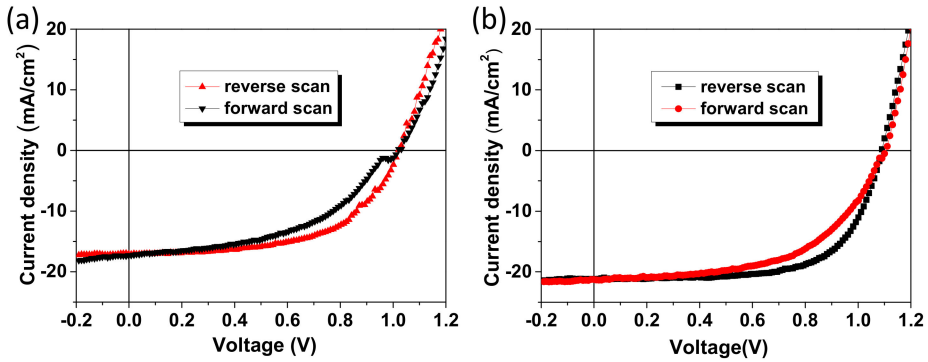

Figure 9. Hysteresis behavior of devices based on TiO_2 ETL without (**a**) and with (**b**) $TiCl_4$ treatment.

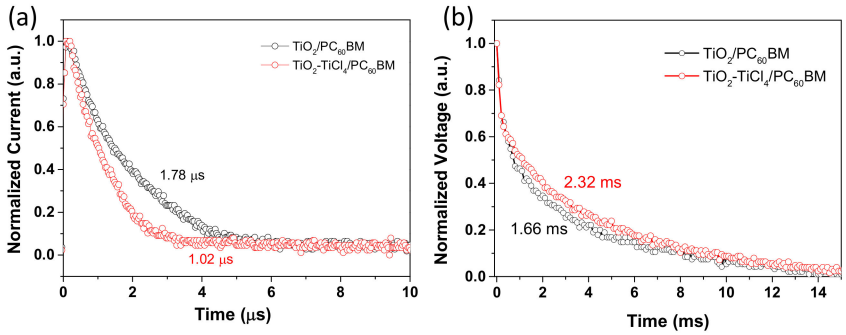

Figure 10. (**a**) Transient photocurrent and (**b**) photovoltage decay characteristics of perovskite solar cells based on TiO_2 ETL with and without $TiCl_4$ treatment.

3. Conclusions

In conclusion, we investigated the effect of $TiCl_4$ treatment on perovskite thin film formation and PSC device performance. The results showed that $TiCl_4$ treatment had a beneficial effect on the properties of perovskite thin film. It could enhance thin film crystallinity and improve charge transfer and extraction. Finally, the PCE was enhanced from 13.2% to 16.5% for devices based on TiO_2 ETL and from 10.2% to 17.0% for devices based on ZnO ETL. This is important for understanding interfacial treatment and further improves device efficiency and stability.

Author Contributions: Conceptualization, Z.L.; methodology, G.L., X.W. and J.D.; validation, J.M.; formal analysis, G.L., M.Z. and J.M.; investigation, G.L., J.D. and Y.G.; resources, X.W., M.Z., and Y.L.; data curation, G.L., X.W. and J.M.; writing—original draft preparation, G.L.; writing—review and editing, Z.L., G.L. and J.M.; visualization, J.D., M.Z., Y.G. and Y.L.; supervision, Z.L.; project administration, Z.L. All authors have read and agreed to the published version of the manuscript.

Funding: This research was funded by National Natural Science Foundation of China, grant number 61604119, 61704131, and 61804111, and the Fundamental Research Funds for the Central Universities.

Conflicts of Interest: The authors declare no conflict of interest.

References

1. Chen, W.; Wu, Y.; Yue, Y.; Liu, J.; Zhang, W.; Yang, X.; Chen, H.; Bi, E.; Ashraful, I.; Grätzel, M.; et al. Efficient and stable large-area perovskite solar cells with inorganic charge extraction layers. *Science* **2015**, *350*, 944–948. [CrossRef] [PubMed]

2. Xing, G.; Mathews, N.; Sun, S.; Lim, S.S.; Lam, Y.M.; Grätzel, M.; Mhaisalkar, S.; Sum, T.C. Long-range balanced electron- and hole-transport lengths in organic-inorganic CH3NH3PbI3. *Science* **2013**, *342*, 344–347. [CrossRef] [PubMed]
3. Shi, D.; Adinolfi, V.; Comin, R.; Yuan, M.; Alarousu, E.; Buin, A.; Chen, Y.; Hoogland, S.; Rothenberger, A.; Katsiev, K.; et al. Low trap-state density and long carrier diffusion in organolead trihalide perovskite single crystals. *Science* **2015**, *347*, 519–522. [CrossRef] [PubMed]
4. Dong, Q.; Fang, Y.; Shao, Y.; Mulligan, P.; Qiu, J.; Cao, L.; Huang, J. Electron-hole diffusion lengths > 175 μm in solution-grown $CH_3NH_3PbI_3$ single crystals. *Science* **2015**, *347*, 967–970. [CrossRef] [PubMed]
5. Stranks, S.D.; Eperon, G.E.; Grancini, G.; Menelaou, C.; Alcocer, M.J.P.; Leijtens, T.; Herz, L.M.; Petrozza, A.; Snaith, H.J. Electron-Hole Diffusion Lengths Exceeding 1 Micrometer in an Organometal Trihalide Perovskite Absorber. *Science* **2013**, *342*, 341–344. [CrossRef] [PubMed]
6. Lee, M.M.; Teuscher, J.; Miyasaka, T.; Murakami, T.N.; Snaith, H.J. Efficient Hybrid Solar Cells Based on Meso-Superstructured Organometal Halide Perovskites. *Science* **2012**, *338*, 643–647. [CrossRef]
7. Yang, W.S.; Park, B.-W.; Jung, E.H.; Jeon, N.J.; Kim, Y.C.; Lee, D.U.; Shin, S.S.; Seo, J.; Kim, E.K.; Noh, J.H.; et al. Iodide management in formamidinium-lead-halide–based perovskite layers for efficient solar cells. *Science* **2017**, *356*, 1376–1379. [CrossRef]
8. Chang, J.; Zhu, H.; Li, B.; Isikgor, F.H.; Hao, Y.; Xu, Q.; Ouyang, J. Boosting the performance of planar heterojunction perovskite solar cell by controlling the precursor purity of perovskite materials. *J. Mater. Chem. A* **2016**, *4*, 887–893. [CrossRef]
9. Chang, J.; Zhu, H.; Xiao, J.; Isikgor, F.H.; Lin, Z.; Hao, Y.; Zeng, K.; Xu, Q.-H.; Ouyang, J. Enhancing the planar heterojunction perovskite solar cell performance through tuning the precursor ratio. *J. Mater. Chem. A* **2016**, *4*, 7943–7949. [CrossRef]
10. Ma, J.; Su, J.; Lin, Z.; Zhou, L.; He, J.; Zhang, J.; Liu, S.; Chang, J.; Hao, Y. Improve the oxide/perovskite heterojunction contact for low temperature high efficiency and stable all-inorganic CsPbI2Br perovskite solar cells. *Nano Energy* **2019**, 104241. [CrossRef]
11. Mo, J.; Zhang, C.; Chang, J.; Yang, H.; Xi, H.; Chen, D.; Lin, Z.; Lu, G.; Zhang, J.; Hao, Y. Enhanced efficiency of planar perovskite solar cells via a two-step deposition using DMF as an additive to optimize the crystal growth behavior. *J. Mater. Chem. A* **2017**, *5*, 13032–13038. [CrossRef]
12. Chang, J.; Lin, Z.; Zhu, H.; Isikgor, F.H.; Xu, Q.-H.; Zhang, C.; Hao, Y.; Ouyang, J. Enhancing the photovoltaic performance of planar heterojunction perovskite solar cells by doping the perovskite layer with alkali metal ions. *J. Mater. Chem. A* **2016**, *4*, 16546–16552. [CrossRef]
13. Jeon, N.J.; Noh, J.H.; Yang, W.S.; Kim, Y.C.; Ryu, S.; Seo, J.; Seok, S. I Compositional engineering of perovskite materials for high-performance solar cells. *Nature* **2015**, *517*, 476–480. [CrossRef] [PubMed]
14. Liu, Z.; Chang, J.; Lin, Z.; Zhou, L.; Yang, Z.; Chen, D.; Zhang, C.; Liu, S.F.; Hao, Y. High-Performance Planar Perovskite Solar Cells Using Low Temperature, Solution-Combustion-Based Nickel Oxide Hole Transporting Layer with Efficiency Exceeding 20%. *Adv. Energy Mater.* **2018**, *8*, 1703432. [CrossRef]
15. Zhou, L.; Chang, J.; Liu, Z.; Sun, X.; Lin, Z.; Chen, D.; Zhang, C.; Zhang, J.; Hao, Y. Enhanced planar perovskite solar cell efficiency and stability using a perovskite/PCBM heterojunction formed in one step. *Nanoscale* **2018**, *10*, 3053–3059. [CrossRef] [PubMed]
16. Zhou, L.; Lin, Z.; Ning, Z.; Li, T.; Guo, X.; Ma, J.; Su, J.; Zhang, C.; Zhang, J.; Liu, S.; et al. Highly Efficient and Stable Planar Perovskite Solar Cells with Modulated Diffusion Passivation Toward High Power Conversion Efficiency and Ultrahigh Fill Factor. *Sol. RRL* **2019**, 1900293. [CrossRef]
17. Wang, S.; Zhang, B.; Feng, D.; Lin, Z.; Zhang, J.; Hao, Y.; Fan, X.; Chang, J. Achieving high performance and stable inverted planar perovskite solar cells using lithium and cobalt co-doped nickel oxide as hole transport layers. *J. Mater. Chem. C* **2019**, *7*, 9270–9277. [CrossRef]
18. Zhang, Z.; Su, J.; Hou, J.; Lin, Z.; Hu, Z.; Chang, J.; Zhang, J.; Hao, Y. Potential Applications of Halide Double Perovskite Cs 2 AgInX 6 (X = Cl, Br) in Flexible Optoelectronics: Unusual Effects of Uniaxial Strains. *J. Phys. Chem. Lett.* **2019**, *10*, 1120–1125. [CrossRef]
19. Lin, Z.; Chang, J.; Xiao, J.; Zhu, H.; Xu, Q.-H.; Zhang, C.; Ouyang, J.; Hao, Y. Interface studies of the planar heterojunction perovskite solar cells. *Sol. Energy Mater. Sol. Cells* **2016**, *157*, 783–790. [CrossRef]
20. Chueh, C.-C.; Li, C.-Z.; Jen, A.K.-Y. Recent progress and perspective in solution-processed Interfacial materials for efficient and stable polymer and organometal perovskite solar cells. *Energy Environ. Sci.* **2015**, *8*, 1160–1189. [CrossRef]

21. Ma, J.; Chang, J.; Lin, Z.; Guo, X.; Zhou, L.; Liu, Z.; Xi, H.; Chen, D.; Zhang, C.; Hao, Y. Elucidating the Roles of TiCl 4 and PCBM Fullerene Treatment on TiO 2 Electron Transporting Layer for Highly Efficient Planar Perovskite Solar Cells. *J. Phys. Chem. C* **2018**, *122*, 1044–1053. [CrossRef]
22. Zhou, Z.; Pang, S.; Liu, Z.; Xu, H.; Cui, G. Interface Engineering for High-Performance Perovskite Hybrid Solar Cells. *J. Mater. Chem. A* **2015**, *3*, 19205–19217. [CrossRef]
23. Fu, F.; Feurer, T.; Jäger, T.; Avancini, E.; Bissig, B.; Yoon, S.; Buecheler, S.; Tiwari, A.N. Low-temperature-processed efficient semi-transparent planar perovskite solar cells for bifacial and tandem applications. *Nat. Commun.* **2015**, *6*, 8932. [CrossRef] [PubMed]
24. Correa Baena, J.P.; Steier, L.; Tress, W.; Saliba, M.; Neutzner, S.; Matsui, T.; Giordano, F.; Jacobsson, T.J.; Srimath Kandada, A.R.; Zakeeruddin, S.M.; et al. Highly efficient planar perovskite solar cells through band alignment engineering. *Energy Environ. Sci.* **2015**, *8*, 2928–2934. [CrossRef]
25. Ke, W.; Fang, G.; Liu, Q.; Xiong, L.; Qin, P.; Tao, H.; Wang, J.; Lei, H.; Li, B.; Wan, J.; et al. Low-Temperature Solution-Processed Tin Oxide as an Alternative Electron Transporting Layer for Efficient Perovskite Solar Cells. *J. Am. Chem. Soc.* **2015**, *137*, 6730–6733. [CrossRef]
26. Li, Y.; Zhao, Y.; Chen, Q.; Yang, Y.; Liu, Y.; Hong, Z.; Liu, Z.; Hsieh, Y.T.; Meng, L.; Li, Y.; et al. Multifunctional Fullerene Derivative for Interface Engineering in Perovskite Solar Cells. *J. Am. Chem. Soc.* **2015**, *137*, 15540–15547. [CrossRef]
27. Ma, J.; Guo, X.; Zhou, L.; Lin, Z.; Zhang, C.; Yang, Z.; Lu, G.; Chang, J.; Hao, Y. Enhanced Planar Perovskite Solar Cell Performance via Contact Passivation of TiO_2/Perovskite Interface with NaCl Doping Approach. *ACS Appl. Energy Mater.* **2018**, *1*, 3826–3834. [CrossRef]
28. Pascual, J.; Kosta, I.; Tuyen Ngo, T.; Chuvilin, A.; Cabanero, G.; Grande, H.J.; Barea, E.M.; Mora-Seró, I.; Delgado, J.L.; Tena-Zaera, R. Electron Transport Layer-Free Solar Cells Based on Perovskite-Fullerene Blend Films with Enhanced Performance and Stability. *ChemSusChem* **2016**, *9*, 2679–2685. [CrossRef]
29. Sandoval-Torrientes, R.; Pascual, J.; García-Benito, I.; Collavini, S.; Kosta, I.; Tena-Zaera, R.; Martín, N.; Delgado, J.L. Modified Fullerenes for Efficient Electron Transport Layer-Free Perovskite/Fullerene Blend-Based Solar Cells. *ChemSusChem* **2017**, *10*, 2023–2029. [CrossRef]
30. Ma, J.; Lin, Z.; Guo, X.; Zhou, L.; Su, J.; Zhang, C.; Yang, Z.; Chang, J.; Liu, S.; Hao, Y. Low-Temperature Solution-Processed ZnO Electron Transport Layer for Highly Efficient and Stable Planar Perovskite Solar Cells with Efficiency Over 20%. *Sol. RRL* **2019**, *3*, 1900096. [CrossRef]
31. You, J.; Meng, L.; Song, T.-B.; Guo, T.-F.; Yang, Y.; Chang, W.-H.; Hong, Z.; Chen, H.; Zhou, H.; Chen, Q.; et al. Improved air stability of perovskite solar cells via solution-processed metal oxide transport layers. *Nat. Nanotechnol.* **2015**, *11*, 75–81. [CrossRef] [PubMed]
32. Zhao, P.; Lin, Z.; Wang, J.; Yue, M.; Su, J.; Zhang, J.; Chang, J.; Hao, Y. Numerical Simulation of Planar Heterojunction Perovskite Solar Cells Based on SnO2 Electron Transport Layer. *ACS Appl. Energy Mater.* **2019**, *2*, 4504–4512. [CrossRef]
33. Zhang, S.; Su, J.; Lin, Z.; Tian, K.; Guo, X.; Zhang, J.; Chang, J.; Hao, Y. Beneficial Role of Organolead Halide Perovskite $CH_3NH_3PbI_3/SnO_2$ Interface: Theoretical and Experimental Study. *Adv. Mater. Interfaces* **2019**, *6*, 1900400. [CrossRef]
34. Guo, X.; Lin, Z.; Ma, J.; Hu, Z.; Su, J.; Zhang, C.; Zhang, J.; Chang, J.; Hao, Y. Low temperature combustion synthesized indium oxide electron transport layer for high performance and stable perovskite solar cells. *J. Power Sources* **2019**, *438*, 226981. [CrossRef]
35. Zhou, L.; Guo, X.; Lin, Z.; Ma, J.; Su, J.; Hu, Z.; Zhang, C.; Liu, S.; Chang, J.; Hao, Y. Interface engineering of low temperature processed all-inorganic CsPbI2Br perovskite solar cells toward PCE exceeding 14%. *Nano Energy* **2019**, *60*, 583–590. [CrossRef]
36. Zhao, P.; Feng, L.; Lin, Z.; Wang, J.; Su, J.; Hu, Z.; Zhang, J.; Ouyang, X.; Chang, J.; Hao, Y. Theoretical Analysis of Two-Terminal and Four-Terminal Perovskite/CIGS Tandem Solar Cells. *Sol. RRL* **2019**, 1900303. [CrossRef]
37. Guo, X.; Zhang, B.; Lin, Z.; Su, J.; Yang, Z.; Zhang, C.; Chang, J.; Liu, S.; Hao, Y. Highly efficient perovskite solar cells based on a dopant-free conjugated DPP polymer hole transport layer: Influence of solvent vapor annealing. *Sustain. Energy Fuels* **2018**, *2*, 2154–2159. [CrossRef]
38. Peng, J.; Wu, Y.; Ye, W.; Jacobs, D.A.; Shen, H.; Fu, X.; Wan, Y.; Duong, T.; Wu, N.; Barugkin, C.; et al. Interface passivation using ultrathin polymer–fullerene films for high-efficiency perovskite solar cells with negligible hysteresis. *Energy Environ. Sci.* **2017**, *10*, 1792–1800. [CrossRef]

39. Liu, Z.; Chen, Q.; Hong, Z.; Zhou, H.; Xu, X.; De Marco, N.; Sun, P.; Zhao, Z.; Cheng, Y.B.; Yang, Y. Low-Temperature TiOx Compact Layer for Planar Heterojunction Perovskite Solar Cells. *ACS Appl. Mater. Interfaces* **2016**, *8*, 11076–11083. [CrossRef]
40. Collavini, S.; Kosta, I.; Völker, S.F.; Cabanero, G.; Grande, H.J.; Tena-Zaera, R.; Delgado, J.L. Efficient Regular Perovskite Solar Cells Based on Pristine [70]Fullerene as Electron-Selective Contact. *ChemSusChem* **2016**, *9*, 1263–1270. [CrossRef]
41. Wojciechowski, K.; Stranks, S.D.; Abate, A.; Sadoughi, G.; Sadhanala, A.; Kopidakis, N.; Rumbles, G.; Li, C.-Z.; Friend, R.H.; Jen, A.K.-Y.; et al. Heterojunction Modification for Highly Efficient Organic–Inorganic Perovskite Solar Cells. *ACS Nano* **2014**, *8*, 12701–12709. [CrossRef] [PubMed]
42. Abdi-Jalebi, M.; Dar, M.I.; Sadhanala, A.; Senanayak, S.P.; Giordano, F.; Zakeeruddin, S.M.; Grätzel, M.; Friend, R.H. Impact of a Mesoporous Titania-Perovskite Interface on the Performance of Hybrid Organic-Inorganic Perovskite Solar Cells. *J. Phys. Chem. Lett.* **2016**, *7*, 3264–3269. [CrossRef] [PubMed]
43. Choe, G.; Kang, J.; Ryu, I.; Song, S.W.; Kim, H.M.; Yim, S. Influence of the concentration of $TiCl_4$ solution used for post-treatment on mesoporous TiO_2 layers in hybrid lead halide perovskite solar cells. *Sol. Energy* **2017**, *155*, 1148–1156. [CrossRef]
44. Murakami, T.N.; Miyadera, T.; Funaki, T.; Cojocaru, L.; Kazaoui, S.; Chikamatsu, M.; Segawa, H. Adjustment of Conduction Band Edge of Compact TiO_2 Layer in Perovskite Solar Cells Through $TiCl_4$ Treatment. *ACS Appl. Mater. Interfaces* **2017**, *9*, 36708–36714. [CrossRef] [PubMed]
45. Chen, H.; Sakai, N.; Ikegami, M.; Miyasaka, T. Emergence of Hysteresis and Transient Ferroelectric Response in Organo-Lead Halide Perovskite Solar Cells. *J. Phys. Chem. Lett.* **2015**, *6*, 164–169. [CrossRef] [PubMed]
46. Meloni, S.; Moehl, T.; Tress, W.; Franckevičius, M.; Saliba, M.; Lee, Y.H.; Gao, P.; Nazeeruddin, M.K.; Zakeeruddin, S.M.; Rothlisberger, U.; et al. Ionic polarization-induced current–voltage hysteresis in CH3NH3PbX3 perovskite solar cells. *Nat. Commun.* **2016**, *7*, 10334. [CrossRef]
47. Almora, O.; Aranda, C.; Zarazua, I.; Guerrero, A.; Garcia-Belmonte, G. Noncapacitive Hysteresis in Perovskite Solar Cells at Room Temperature. *ACS Energy Lett.* **2016**, *1*, 209–215. [CrossRef]
48. Zhao, C.; Chen, B.; Qiao, X.; Luan, L.; Lu, K.; Hu, B. Revealing Underlying Processes Involved in Light Soaking Effects and Hysteresis Phenomena in Perovskite Solar Cells. *Adv. Energy Mater.* **2015**, *5*, 1500279. [CrossRef]